Jour. Fac. Sci., Hokkaido Univ., Ser. VII (Geophysics), Vol. 8, No. 3, 191-208, 1988.

SH-Waves in a Laterally Varying Medium : (1) The Seismic Response of Sediment-Filled Valleys to Plane-Incident *SH*-Waves

Tsutomu Sasatani

Department of Geophysics, Faculty of Science, Hokkaido University, Sapporo 060, Japan

(Received Nov. 2, 1987)

Abstract

We applied the discrete wavenumber method proposed by Campillo and Bouchon (1985) to computation of the *SH* wavefield produced by incident plane waves in a laterally varying medium. After various tests of the accuracy of this method for simple problems, we systematically investigated the response of sediment-filled valleys to plane-incident *SH* waves. The valley was assumed to consist of a layer and a half-space separated by a one cycle cosine-shaped interface. The main effect induced by boundary curvature is the generating of Love waves on the dipping interface and their subsequent trapping inside the valley. This effect strongly depends on the shape ratio (sediment thickness to valley half-width ratio), the velocity contrast between the sediment and the underlying bedrock, and incident wavefield characteristics. For a deep valley with a high velocity contrast, Love waves are efficiently generated and reflected at the valley edges, resulting in a large amplification and in a long duration of the ground shaking inside the valley. These outcomes show that the flat layer theory appears strongly inadequate to compute reliable ground motions.

1. Introduction

It is well established that alluvial valleys and sedimentary basins are generally exposed to seismic motion amplification, and that signal records are longer and more complex on such sites than on crystalline rocks (e.g., King and Tucker, 1984; Kudo and Sakaue, 1984; Okada and Kagami, 1978). These phenomena are considered to be induced by the focusing of seismic rays and surface wave generation in a laterally varying medium. Figure 1 shows an example of such phenomena. Hiroo strong-motion record is particularly simple, while Obihiro record is more complex and has a long duration of the ground shaking. Obihiro is located near the center of the sedimentary basin in Tokachi

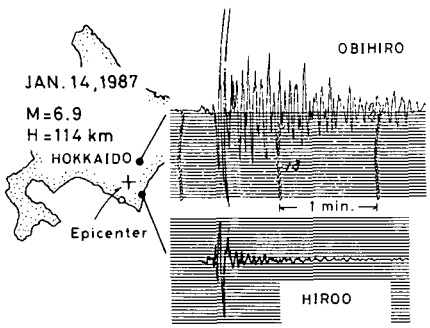

Fig. 1 JMA strong-motion (displacement) seismograms showing significant differences in site responses.

plain and Hiroo, at the edge of the basin. Thus, the contrast between the strong-motion records in Fig. 1 has been interpreted to be due to the basin effects (Sasatani, 1985, 1987).

For a long time, studies of the basin or valley effects on the ground motion have been essentially qualitative. Recently, several attempts have been made to compute such effects theoretically by using various methods (Aki and Larner, 1970 ; Bard and Bouchon, 1980, 1985 ; Boore et al., 1971 ; Horike, 1987 ; Kohketsu, 1987 ; Nowack and Aki, 1984). The quantitative comparison between observational and theoretical results has just begun (Cohn et al., 1982 ; Sasatani, 1987 ; Zama, 1981).

The purpose of the present study is to investigate systematically the seismic response of sediment-filled valleys to plane-incident *SH* waves. A similar study has been done by Bard and Bouchon (1980) by means of the Aki-Larner method, which becomes inappropriate for high frequencies. Here we use the discrete wavenumber method proposed by Campillo and Bouchon (1985) to calculate the response. This method is applicable to boundaries of arbitrary shapes and is valid at all frequencies. First, we represent the method to calculate the *SH* wavefield produced by incident plane waves in a laterally varying medium. After various tests of the accuracy of the method, we systematically investigate the response of sediment-filled valleys. We will see a similar contrast as shown in Fig. 1 between the synthetic seismograms at the valley center and at the edge.

2. Method

We consider the two-dimensional problem of the response of an irregularly

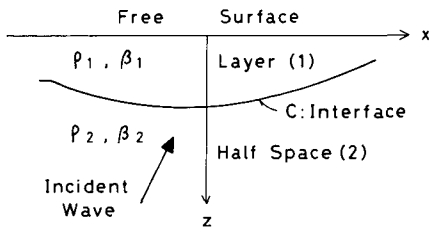

Fig. 2 Geometry of the problem. The interface C has an arbitrary shape.

layered elastic medium to an incident plane SH-wave. We assume the medium to consist of a layer and a half-space separated by an irregular interface C (Fig. 2). The interface depth C is a function of x alone. β_1, ρ_1 and β_2, ρ_2 are respectively the wave velocity and the density of the layer (1) and of the half-space (2). For the incident wave in the half-space, the displacement at a location $r(x, z)$ may be expressed as:

$$\begin{aligned} V^{(1)}(x, z) &= V_c^{(1)}(x, z) \quad ; r\in(1) \\ V^{(2)}(x, z) &= V_c^{(2)}(x, z) + V_I(x, z) \; ; r\in(2) \end{aligned} \tag{1}$$

where $V_c^{(i)}$ represents the displacement associated with the field diffracted at the interface in medium (i). V_I denotes the displacement due to the incident wave and can be written as:

$$V_I(x, z) = \exp[-ik_0 x + i\gamma_0 z] \; ; \; r\in(2) \tag{2}$$

where

$$k_0 = \frac{\omega}{\beta_2} \sin\theta,$$

$$\gamma_0 = \left(\frac{\omega^2}{\beta_2^2} - k_0^2\right)^{1/2} = \frac{\omega}{\beta_2} \cos\theta,$$

θ is an incident angle and ω, an angular frequency. Note that for briefness, the time dependence $\exp(i\omega t)$ is omitted throughout the analysis.

The diffracted field $V_c^{(i)}$ may be represented by the radiation of a specified distribution of seismic sources (forces)$F^{(i)}$ along C (Huygens' principle). This representation will be exact for the entire zone (i) if the radiation is calculated with an accurate Green's function and if the boundary conditions are satisfied on C. For region (1) the homogeneous half-space Green's function is required, while the infinite space Green's function is required for region (2).

The source distributions $F^{(1)}$ and $F^{(2)}$ on C are determined by the boundary conditions, the displacement and stress continuity conditions, at the interface

itself. The boundary conditions are, for any (x, z) on C:

$$\begin{aligned} &V^{(1)}(x, z)= V^{(2)}(x, z) \\ &\mu_1\left[n_x \frac{\partial V^{(1)}(x, z)}{\partial x}+n_z \frac{\partial V^{(1)}(x, z)}{\partial z}\right] \\ &=\mu_2\left[n_x \frac{\partial V^{(2)}(x, z)}{\partial x}+n_z \frac{\partial V^{(2)}(x, z)}{\partial z}\right] \end{aligned} \tag{3}$$

where μ_1 and μ_2 are the rigidities in mediums (1) and (2), and $\boldsymbol{n}(n_x, n_z)$ represents the normal vector to C at $r(x, z)$. n_x and n_z are, according to Aki and Larner (1970),

$$\begin{aligned} n_x&=-\left(\frac{dC}{dx}\right)\left[1+\left(\frac{dC}{dx}\right)^2\right]^{-1/2}, \\ n_z&=\left[1+\left(\frac{dC}{dx}\right)^2\right]^{-1/2}. \end{aligned} \tag{4}$$

Assuming that $G^{(1)}(x, z ; x', z')$ and $G^{(2)}(x, z ; x', z')$ are the Green's functions for regions (1) and (2), equation (1) is given by:

$$\begin{aligned} V^{(1)}(x, z)&=\int_c F^{(1)}(x', z')G^{(1)}(x, z ; x', z')d\xi \\ V^{(2)}(x, z)&=\int_c F^{(2)}(x', z')G^{(2)}(x, z ; x', z')d\xi+V_I(x, z) \end{aligned} \tag{5}$$

with $\xi=(x', z')$. The use of these expressions in equations (3) yields two integral equations which give theoretically the distributions $F^{(1)}$ and $F^{(2)}$ through the Green's functions and their spatial derivatives.

In order to solve the integral equations, we have to discretize the integrals over C and to evaluate the Green's functions. To this we assume that the source-medium configuration is periodic in the x-direction with a spatial periodicity L (Fig. 3), and that the irregular interface may be represented by an array of $2M+1$ discrete points regularly spaced in x (Fig. 3), where forces are applied and where the boundary conditions are matched. The value of M is

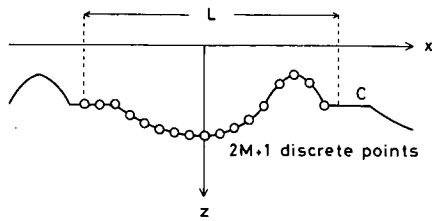

Fig. 3 Introduction of a periodicity in the medium geometry and discretization of the interface at regular sapcing.

chosen such that the following condition of sampling is satisfied: $L/(2M+1)<\pi\beta'/\omega=\lambda'/2$ where β' is the lowest wave velocity of the medium and λ' is the shortest wavelength. Using the discrete wavenumber method based on these assumptions (Campillo and Bouchon, 1985), we can evaluate the displacements produced by the entire distribution $F_m^{(i)}(x_m, z_m)$ $(m=-M\sim M)$ in medium (i). They are:

$$\begin{aligned} V_c^{(1)}(x_j, z)=&\frac{1}{2i\mu_1 L}\sum_{m=-M}^{M}F_m^{(1)}\sum_{p=-M}^{M}\frac{1}{\gamma_p^{(1)}}\\ &\cdot\{\exp[-\gamma_p^{(1)}|z-z_m|-ik_p(x_j-x_m)]\\ &+\exp[-\gamma_p^{(1)}(z+z_m)-ik_p(x_j-x_m)]\} \qquad (6)\\ V_c^{(2)}(x_j, z)=&\frac{1}{2i\mu_2 L}\sum_{m=-M}^{M}F_m^{(2)}\sum_{p=-M}^{M}\frac{1}{\gamma_p^{(2)}}\\ &\cdot\exp[-i\gamma_p^{(2)}|z-z_m|-ik_p(x_j-x_m)] \end{aligned}$$

where

$$k_p=p\frac{2\pi}{L},\quad \gamma_p^{(1)}=\left(\frac{\omega^2}{\beta_1^2}-k_p^2\right)^{1/2},\quad Im(\gamma_p^{(1)})\leq 0,$$
$$\gamma_p^{(2)}=\left(\frac{\omega^2}{\beta_2^2}-k_p^2\right)^{1/2},\quad Im(\gamma_p^{(2)})\leq 0.$$

To obtain these expressions, we utilized the infinite space Green's function (Lamb, 1904), that is, the *SH* displacement V produced at $r(x, z)$ by a transverse line force F acting at (x', z'):

$$V(x, z)=\frac{F}{4\pi\mu i}\int_{-\infty}^{+\infty}\frac{1}{\gamma}\exp[-ik(x-x')-i\gamma|z-z'|]dk \qquad (7)$$

with

$$\gamma=\left(\frac{\omega^2}{\beta^2}-k^2\right)^{1/2},\quad Im(\gamma)\leq 0.$$

Using the expressions (6) in equation (3) and writing the boundary conditions at each points of the contour C leads to a system of $4M+2$ linear equations in $F_m^{(i)}$:

$$\left(\begin{array}{c|c}\boldsymbol{A}^{(1)} & \boldsymbol{A}^{(2)}\\ \hline \boldsymbol{B}^{(1)} & \boldsymbol{B}^{(2)}\end{array}\right)\left(\begin{array}{c}F_m^{(1)}\\ \hline F_m^{(2)}\end{array}\right)=\left(\begin{array}{c}D_j^{(2)}\\ \hline S_j^{(2)}\end{array}\right);\quad m, j=-M\sim M \qquad (8)$$

The elements of partitioned matrices are as follows:

$$\begin{aligned} A_{jm}^{(1)}=&\frac{1}{2i\mu_1 L}\sum_{p=-M}^{M}\frac{1}{\gamma_p^{(1)}}\{\exp[-i\gamma_p^{(1)}|z_j-z_m|-ik_p(x_j-x_m)]\\ &+\exp[-i\gamma_p^{(1)}(z_j+z_m)-ik_p(x_j-x_m)]\} \end{aligned}$$

$$A_{jm}^{(2)}=\frac{-1}{2i\mu_2 L}\sum_{p=-M}^{M}\frac{1}{\gamma_p^{(2)}}\exp[-i\gamma_p^{(2)}\mid z_j-z_m\mid-ik_p(x_j-m_m)]$$

$$B_{jm}^{(1)}=\frac{1}{2L}\sum_{p=-M}^{M}\left\{\left[-n_x\frac{k_p}{\gamma_p^{(1)}}+\varepsilon_1 n_z\right]\exp[-i\gamma_p^{(1)}\mid z_j-z_m\mid-ik_p(x_j-x_m)]\right.$$
$$\left.+\left[-n_x\frac{k_p}{\gamma_p^{(1)}}-n_z\right]\exp[-i\gamma_p^{(1)}(z_j+z_m)-ik_p(x_j-x_m)\right\} \qquad (9)$$

$$B_{jm}^{(2)}=\frac{-1}{2L}\sum_{p=-M}^{M}\left[-n_x\frac{k_p}{\gamma_p^{(2)}}+\varepsilon_2 n_z\right]\exp[-i\gamma_p^{(2)}\mid z_j-z_m\mid-ik_p(x_j-x_m)]$$

$$D_j^{(2)}=\exp[-i\gamma_0\mid z_j-z_{ref}\mid-ik_0x_j]$$

$$S_j^{(2)}=i\mu_2[-n_xk_0+n_z\gamma_0]\exp[-i\gamma_0\mid z_j-z_{ref}\mid-ik_0x_j]$$

where

$$\varepsilon_1=\begin{cases}+1\\+1\\-1\end{cases}\quad\text{and}\quad\varepsilon_2=\begin{cases}+1 & \text{for } z_j<z_m\\-1 & \text{for } z_j=z_m\\-1 & \text{for } z_j>z_m\end{cases}$$

and z_{ref} is a reference level for the phase which is chosen below the deepest point on C. After resolution of this system we are able to evaluate the elastic field anywhere in the medium using equation (6). The calculation is made for each frequency and the results are synthesized in the time domain by the inverse Fourier transform. To avoid the unwanted effect of source-medium periodicity, we give to the frequency an imaginary part. Its attenuation effect is later removed from the time domain solution (Bouchon, 1979).

3. Tests of the method

As a way to test the accuracy of our approach we compute synthetic seismograms for simple three cases ((1) a single plane interface, (2) a flat layer over a half-space, and (3) a soft basin model), and we compare them with the results obtained by the different methods.

3.1 A single plane interface

This corresponds to the plane-wave reflection and transmission problem at a plane interface. Their coefficients are given by analytical expressions and are frequency independent (e.g., Aki and Richards, 1980). The source-receiver configuration and the synthetic seismograms obtained by our technique are displayed in Fig. 4. In this case the infinite space Green's function is required for region (1) as well as for region (2). As incident signal, we take a one cycle sine wave with a period of 2 sec. The weveshapes of the transmitted and

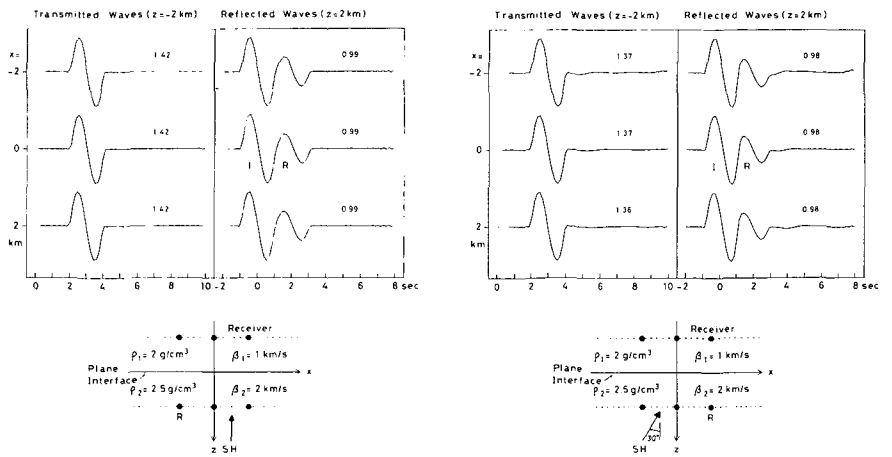

Fig. 4 Source-receiver geometry and synthetic seismograms for a single plane-interface problem. (a) Vertical and (b) oblique incidences. Numbers attached to each trace indicate the peak to peak amplitude, while incident signal has the unit amplitude. In the traces for reflected waves, the first disturbance corresponds to incident signal denoted by I.

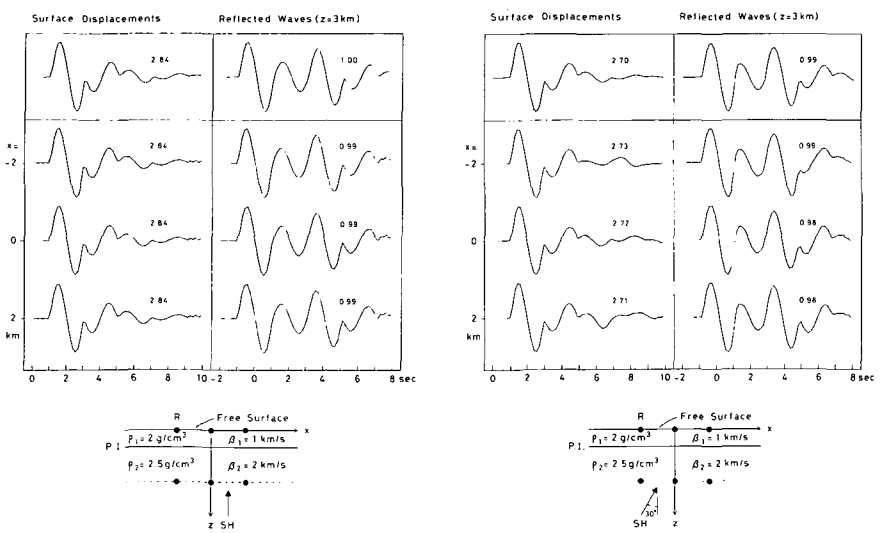

Fig. 5 Source-receiver geometry of a flat layer over a half-space model and comparison between our results (lower traces) and synthetic seismograms obtained by the propagator matrix method (uppermost traces). (a) Vertical and (b) oblique incidences. Notations are the same as those in Fig. 4.

reflected waves and their amplitudes are in good agreement with the theoretical results for both vertical and oblique incidences.

3.2 A flat layer over a half-space

The geometry and the parameters of the medium are shown in Fig. 5. The synthetic seismograms obtained by our technique are compared with the results obtained by the propagator-matrix method (Aki and Richards, 1980) in the figure. The incident signal is identical with that used in the previous calculations. An agreement between the traces obtained by the two methods is good for both the surface displacements and the reflected waves. This indicates that our technique takes well vertical interferences into account.

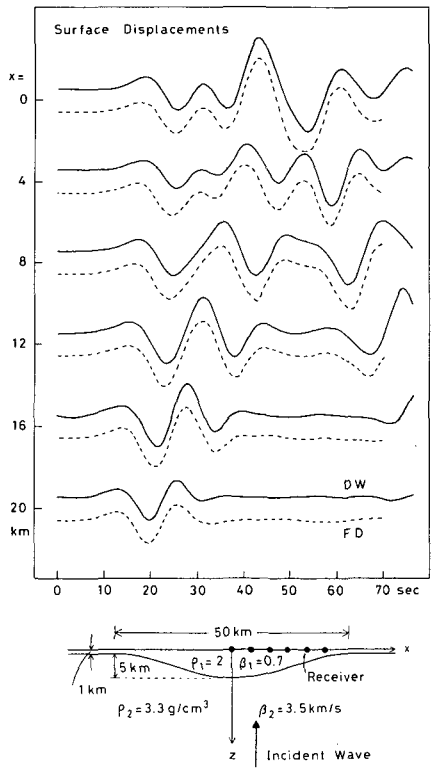

Fig. 6 Source-receiver geometry of a soft basin model and comparison between our results (DW) and those of finite difference method (FD ; Boore et al., 1971). The traces are the surface displacement at six sites located at a horizontal distance of 0 to 20 km from the basin center.

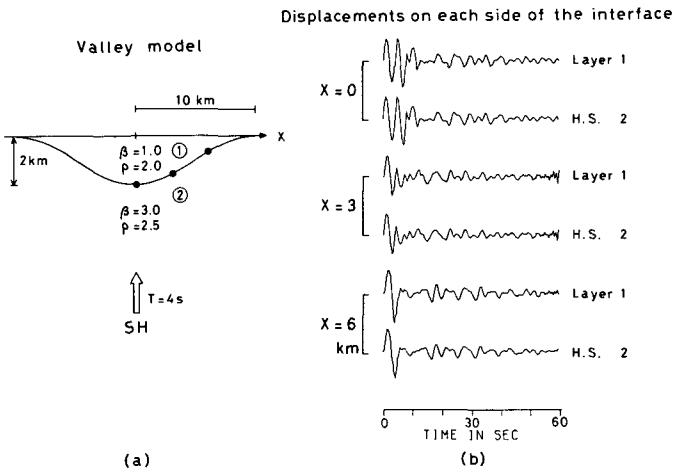

Fig. 7 Comparison of displacements obtained at three couples of points on each side of the interface. The upper trace is inside the valley, and the lower one is in the half-space. The characteristics of the valley and of the incident signal are specified on the figure.

3.3 A soft basin model

As a final example of the test, we consider the response of a one cycle cosine-shaped basin to a vertically incident *SH* wave. The geometry and the parameters of the medium are shown in Fig. 6. This problem has been first studied by Boore et al. (1971) using a finite difference (FD) technique. We compare the synthetic seismograms at various sites along the free surface with the results obtained by Boore et al. (1971) in Fig. 6. As incident signal, a Ricker wavelet with a characteristic period of 18.3 sec is taken (Bard and Bouchon, 1980). The comparison shows a good agreement of our method (DW) with FD method.

Furthermore, to test reliability of our method, we compare displacements on each side of the interface in the time domain in Fig. 7. The characteristics of the basin are specified on the figure. Here, a one cycle sine wave with a period of 4 sec is taken as incident signal. The good matching of one of the boundary conditions (3) can be seen at three couples of points.

These various tests show the validity of our approach.

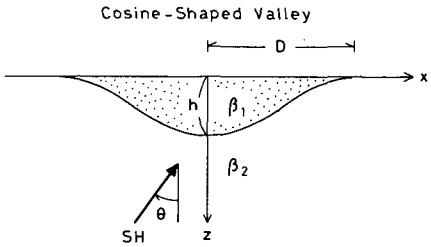

Fig. 8 Geological configuration of sediment-filled valleys with a one cycle cosine-shaped interface. D is the valley half-width and h, the maximum depth.

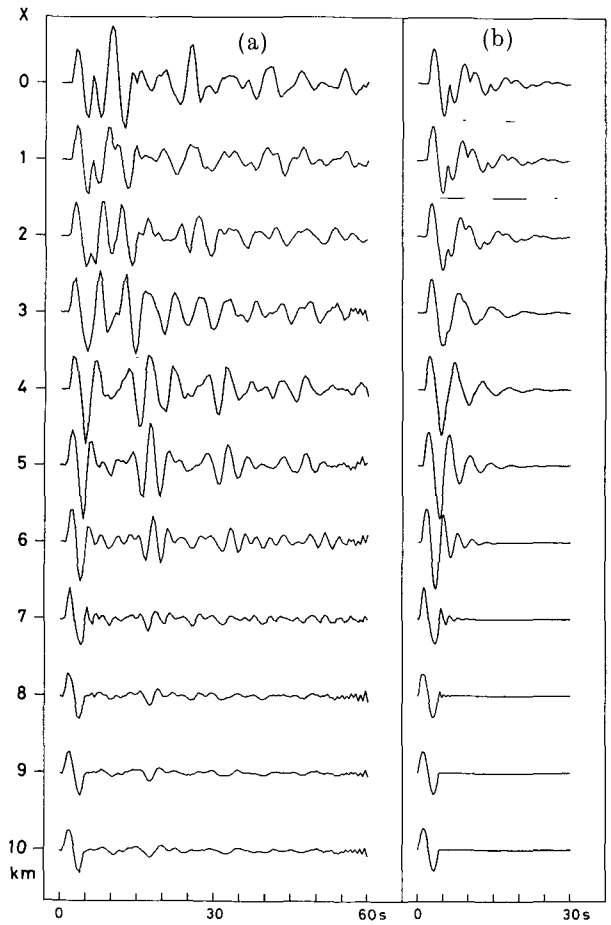

Fig. 9 (a) Response of a sediment-filled valley to a vertically incident SH wave. The valley characteristics are the same as in Fig. 7. The traces represent the displacement at surface receivers, spaced from 0 to 10 km from the valley center. (b) Responses derived from the flat-layer approximation. Incident signal is a one cycle sine wave with a period of 4 sec. Only one side of the valley is represented because of the symmetry of the problem.

4. Responses of sediment-filled valleys

In this section we study the responses of sediment filled valleys to incident plane *SH* waves. We consider a one cycle cosine-shaped interface defined by

$$C(x)=\frac{h}{2}\left(1+\cos\frac{\pi x}{D}\right) \qquad \text{for } |x|<D$$
$$C(x)=0 \qquad \text{for } |x|>D$$

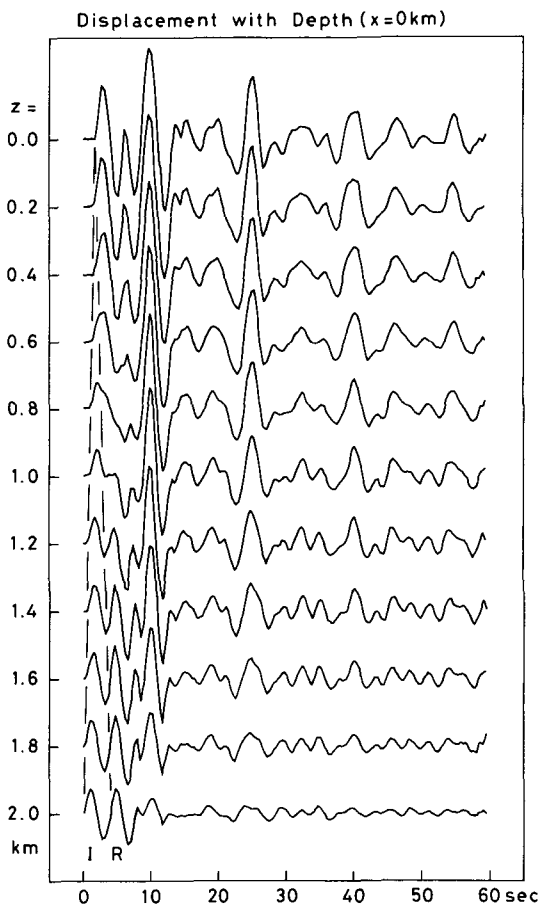

Fig. 10 Evolution of the displacement with depth at the valley center. The valley characteristics are the same as in Fig. 7. The uppermost trace ($z=0$ km) corresponds to the surface displacement and the last trace ($z=2$ km), to the interface displacement. I indicates the incident *SH* wave and R, the reflected *SH* wave.

where D is the valley half-width and h, the maximum depth (Fig. 8; Bard and Bouchon, 1980). First, we show general features of the responses of sediment-filled valleyes, comparing them with the responses by the flat-layer approximation.

Figure 9(a) shows the displacement response of a valley to a vertically incident SH wave. The geometry and the parameters of the medium are shown in Fig. 7(a). Only one side of the valley is represented because of the symmetry of the problem. The valley response shows, in addition to the direct SH wave, the generation of waves on the dipping interfaces, and their subsequent lateral propagation toward the other edge. These local surface waves (i.e., Love waves) can be reflected several times on the raising interface, resulting in a long duration of the ground shaking inside the valley. The amplitude of Love waves depends on the site location inside the valley, and the meeting of waves generated at each edge produces a strong amplification in the center of the valley.

To further investigate the nature of these waves we look at the evolution of displacement with depth at the center of the valley in Fig. 10. We can see the upgoing (incident wave denoted by I) and downgoing (reflected wave denoted by R) SH-waves during the first several seconds of the seismograms. The disturbances that follow these SH-waves have no phase shift with depth and exhibit

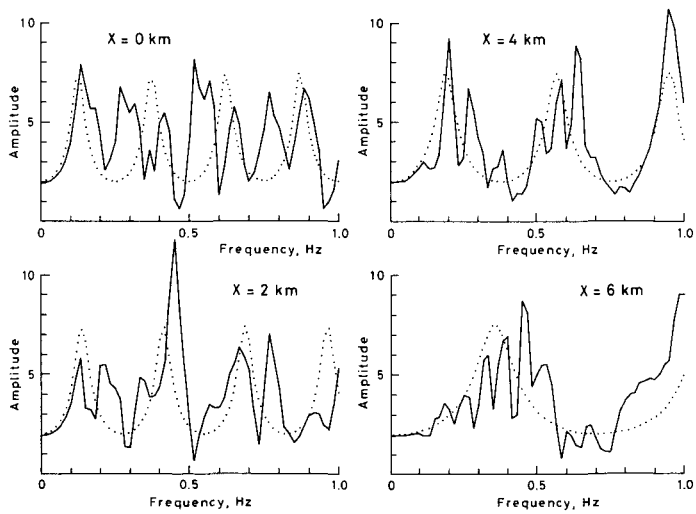

Fig. 11 Comparison between the valley (solid line) and the flat-layer (dotted line) spectral transfer functions at four surface sites. The valley characteristics are the same as in Fig. 7.

the cosine dependence of the amplitude versus depth curve. These facts confirm that the elastic wavefield induced in the valley is composed of fundamental Love modes (Bard and Bouchon, 1980).

Figure 9(b) shows the flat-layer responses calculated assuming, at each point, that the valley structure is a horizontal layer having a constant thickness equal to that directly beneath the point. Comparing them with Fig. 9(a), we can see that the flat-layer approximation is valid only during the first one cycle of the disturbance, and that a striking discrepancy between the valley and flat-layer responses appears at later times. We cannot predict the long duration of the ground shaking inside the valley by the flat-layer approximation. Figure 11 shows the frequency domain behaviour corresponding to Fig. 9 for several points located at the surface of the valley. The discrepancy between two responses is

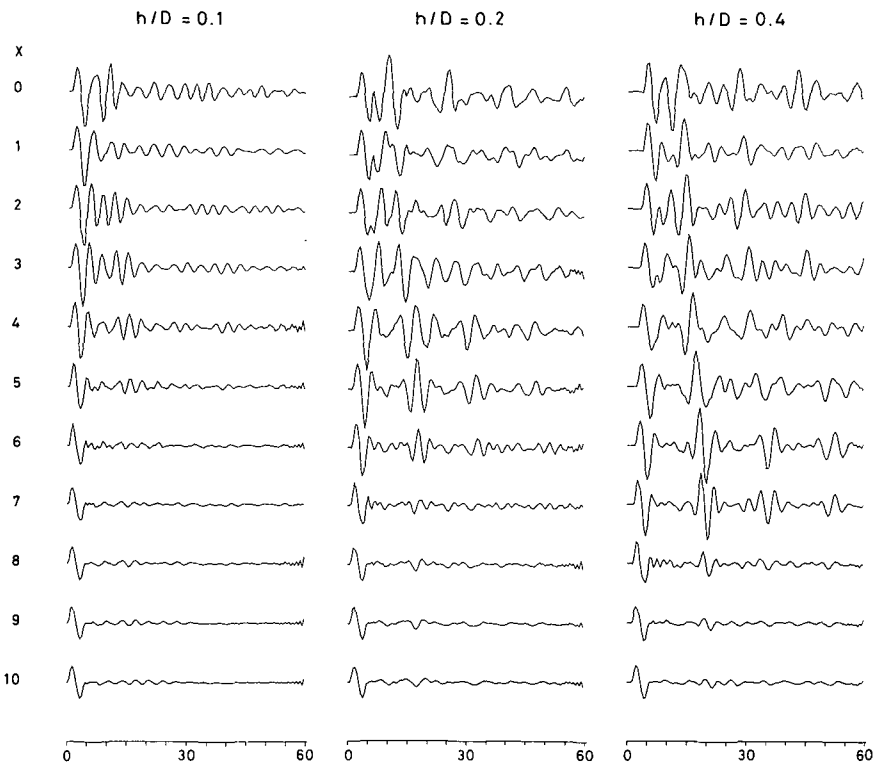

Fig. 12 Effects of the shape ratio on the valley response at surface receivers. Three different shape ratios ($h/D=0.1$, 0.2 and 0.4) are considered by changing the maximum depth (h). The other parameters are: $D=10$ km, $VC=3$ ($\beta_1=1$ km/sec, $\beta_2=3$ km/sec), $\theta=0°$, and $T=4$ sec.

also evident in the frequency domain. These demonstrate that the "classical" flat-layer approximation is inadequate to calculate the response of a nonplanar layered structure such as a sediment-filled valley.

Bard and Bouchon (1980) noted that the valley responses were influenced by the valley parameters and incident wavefield characteristics. Then we systematically investigate the effects of the shape ratio (h/D ; the ratio of the maximum sediment thickness to the valley half-width), the velocity contrast ($VC=\beta_2/\beta_1$), the incident angle (θ) and the spectrum of incident signal on the valley responses. In the investigation, we compare the synthetic seismograms calculated for several combinations of the parameters, which are given in each figure caption. As incident signal, we take a one cycle sine wave with a period of T.

Effect of shape ratio. The effect of shape ratio is illustrated in Fig. 12. For

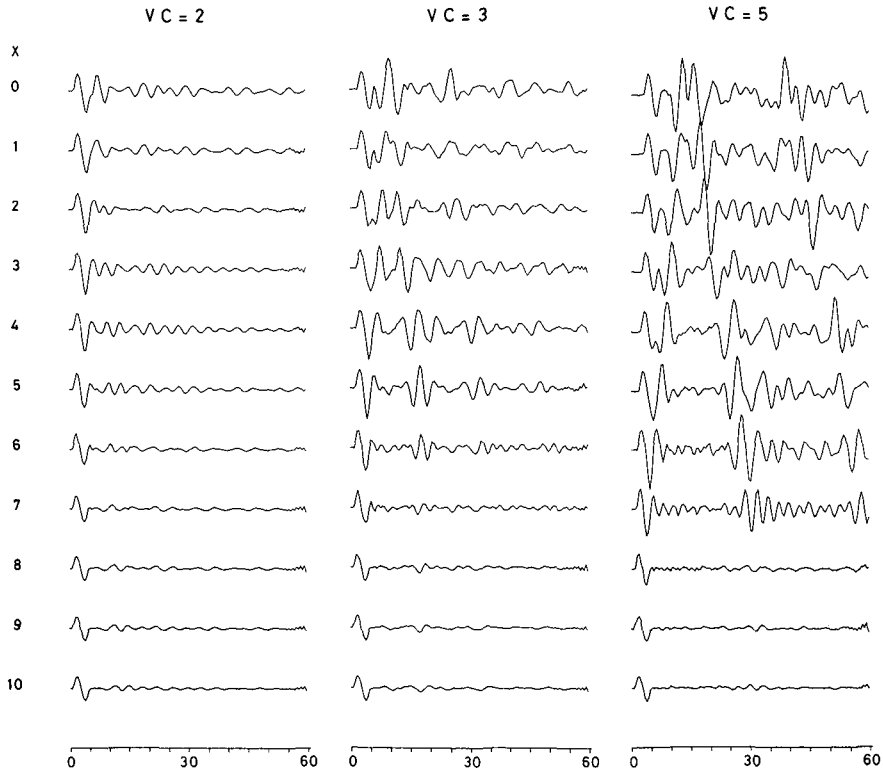

Fig. 13 Effects of the velocity contrast on the valley response at surface receivers. Three different velocity contrasts ($VC=2$, 3 and 5) are considered by changing the sediment velocity (β_1). The other parameters are: $h/D=0.2$ ($D=10$ km, $h=2$ km), $\beta_2=3$ km/sec, $\theta=0°$, and $T=4$ sec.

deeper valleys, the Love wave amplitudes are greater than those for shallow valleys. The zone within which Love waves propagate becomes wider with the shape ratio. These indicate that the amount of energy reflected on the interface increases with the interface mean slope. The dispersion pattern of Love waves depends on the shape ratio.

Effect of velocity contrast. Figure 13 shows the effect of velocity contrast. For higher velocity contrast, Love waves are efficiently reflected at the edge and hence, have much larger amplitude than the disturbance associated with the direct incident signal. These effects are similar to those induced by deeper valleys and result in a long duration of the ground shaking in the valley in the presence of the high velocity contrast. For the low contrast ($VC=2$), the peak

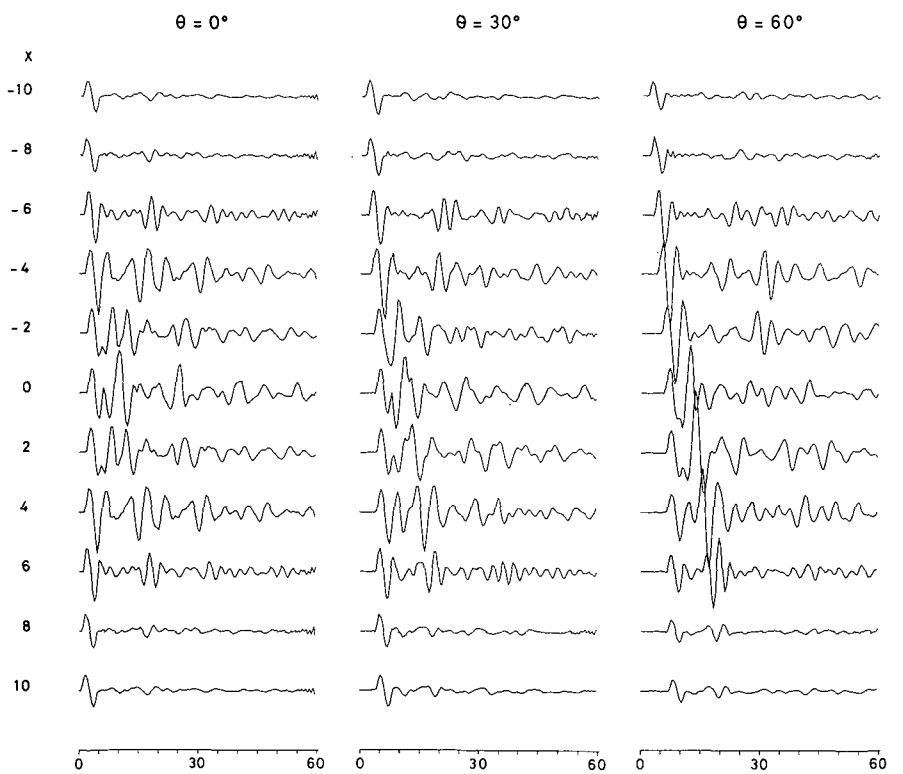

Fig. 14 Effects of the incident angle on the valley response at surface receivers. Three different incident angles are considered: $\theta=0°$, 30°, and 60°. The other parameters are: $h/D=0.2$ ($D=10$ km, $h=2$ km), $VC=3$ ($\beta_1=1$ km/sec, $\beta_2=3$ km/sec), and $T=4$ sec. The whole valley is now illustrated since the problem is no longer symmetrical.

amplitude at each point is now always recorded at the direct arrival of the incident signal, but the Love wave generation and propagation are still clear.

Effect of incident angle. When the waves are obliquely incident, the problem configuration is no longer symmetric. Then the responses are illustrated for the whole valley in Fig. 14, which clearly shows the asymmetry of the oblique incidence case. Another effect of oblique incidence is the shifting of the zone where maximum surface displacement occurs.

Effect of spectrum of incident signal. We investigate the effect of the spectrum of incident signal by changing the period of incident signal for a deep valley ($h/D=0.4$) with a high velocity contrast ($VC=5$). Figure 15 shows that the peak amplitude significantly increases with the period of incident signal. This may be due to the two-dimensional resonance pattern (vertical and lateral interfer-

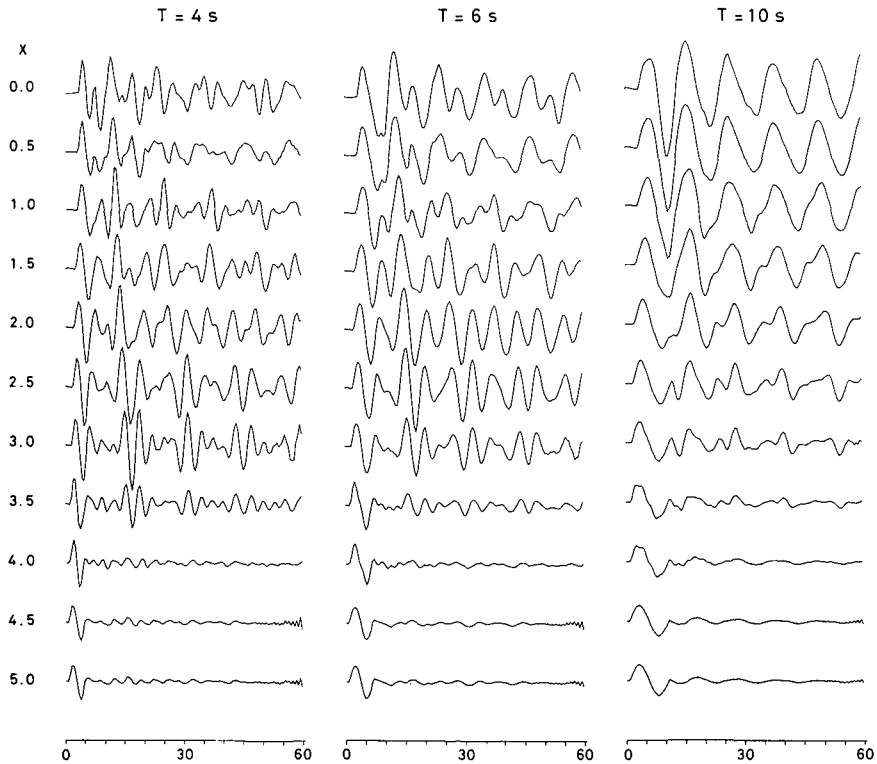

Fig. 15 Effects of the period of incident signal on the valley response at surface receivers. Three different periods are considered: $T=4$, 6, and 10 sec. The other parameters are: $h/D=0.4$ ($D=5$ km, $h=2$ km), $VC=5$ ($\beta_1=0.6$ km/sec, $\beta_2=3$ km/sec), and $\theta=0°$.

ences) as demonstrated by Bard and Bouchon (1985). In fact, the longest period (10 sec) we used is close to the fundamental resonance period of the valley considered, which is 12.4 sec according to their result in the antiplane (*SH*) case. Moreover, the ground motion is approximately in phase across a half of the valley for $T=10$ sec. The two-dimensional resonance of sediment-filled valleys has been studied in detail by Bard and Bouchon (1985).

5. Concluding remarks

The study of the *SH* response of sediment-filled valleys by using the method proposed by Campillo and Bouchon (1985) shows that the main effect induced by boundary curvature is the generating of Love waves on the dipping interface and their subsequent trapping inside the valley. For deeper valleys with a high velocity contrast, Love waves are efficiently generated and reflected at the valley edges, resulting in a strong amplification and in a long duration of the ground shaking inside the valley.

Although our results are restricted to the teleseismic domain because of the assumed planarity of the incident wave field, one may quite reasonably apply them to the valley response in case of near-by deep earthquakes. In fact, the synthetic seismograms at the valley center and at the edge (e.g., Fig. 9(a)) show a similar contrast as observed in Fig. 1.

Our results have been obtained for a very simple valley shape, that is, a one cycle cosine-shaped valley. The actually existing valley may have a more irregular interface. For such a valley, our results suggest that the response becomes moreover complex. Then the reliable prediction of strong ground motion from earthquakes requires the detailed structure of the sediment-filled valley.

Acknowledgments

The numerical calculations were carried out by HITAC M-280 H at the Hokkaido University Computing Center.

References

Aki, K. and K.L. Larner, 1970. Surface motion of a layered medium having an irregular interface due to incident plane *SH* waves. J. Geophys. Res., **75**, 933-954.

Aki, K. and P.G. Richards, 1980. Quantitative seismology : Theory and methods, vol. 1, pp. 1-

557, W.H. Freeman and Company.
Bard, P.-Y. and M. Bouchon, 1980. The seismic response of sediment-filled valleys. Part 1. The case of incident *SH* waves. Bull. Seism. Soc. Am., **70**, 1263-1286.
Bard, P.-Y. and M. Bouchon, 1985. The two-dimensional response of sediment-filled valleys. Bull. Seism. Soc. Am., **75**, 519-541.
Boore, D.M., K.L. Larner and K. Aki, 1971. Comparison of two independent methods for the solution of wave-scattering problems: response of a sedimentary basin to vertically incident *SH* waves. J. Geophys. Res., **76**, 558-569.
Bouchon, M., 1979. Discrete wave number representation of elastic vave-fields in three-space dimensions. J. Geophys. Res., **84**, 3609-3614.
Campillo, M. and M. Bouchon, 1985. Synthetic *SH* seismograms in a laterally varying medium by the discrete wavenumber method. Geophys. J.R. astr. Soc., **83**, 307-317.
Cohn, S.N., T.L. Hong and D.V. Helmberger, 1982. The Oroville earthquakes: A study of source characteristics and site effects. J. Geophys. Res., **87**, 4585-4594.
Horike, M., 1987. Extension of the Aki and Larner method to absorbing media with plural curved interfaces and several characteristics of a seismic response on a sedimentary basin. Zisin (J. Seism. Soc. Japan), **40**, 247-259 (in Japanese).
King, J.L. and B.E. Tucker, 1984. Observed variation of earthquake motion across a sediment-filled valley. Bull. Seism. Soc. Am., **74**, 137-151.
Kohketsu, K., 1987. 2-D reflectivity method and synthetic seismograms for irregularly layered structures — I. *SH*-wave generation. Geophys. J.R. astr. Soc., **89**, 821-838.
Kudo, K. and M. Sakaue, 1984. Oil-sloshing in the huge tanks at Niigata due to the Nihonkai-Chubu earthquake of 1983. Bull. Earthq. Res. Inst., Univ. Tokyo, **59**, 361-382 (in Japanese).
Lamb, H., 1904. On the propagation of tremors at the surface of an elastic solid. Phil. Trans. Roy. Soc. London, Ser. A, **203**, 1-42.
Nowack, R. and K. Aki, 1984. The two-dimensional Gaussian beam synthetic method: testing and application. J. Geophys. Res., **89**, 7797-7819.
Okada, S. and H. Kagami, 1978. A point-by-point evaluation of amplification characteristics in Japan on 1-10 sec seismic motions in relation to deep soil deposits. Trans. Archi. Inst. Japan, **265**, 29-38 (in Japanese).
Sasatani, T., 1985. A study of the strong ground motion of the western Hidaka, Hokkaido earthquake. Geophys. Bull. Hokkaido Univ., **46**, 69-83 (in Japanese).
Sasatani, T., 1987. A study of the strong ground motion from intermediate-depth earthquakes. Geophys. Bull. Hokkaido Univ., **49**, 63-73 (in Japanese).
Zama, S., 1981. Behaviour of the elastic wave propagating through the irregular structures. II. Damage at Asaba-Cho in the lower reaches of the Ohta river in Shizuoka prefecture due to the 1944 Tonankai earthquake. Bull. Earthq. Res. Inst., Univ. Tokyo, **56**, 753-760 (in Japanese).